

Rossby numbers of fully and partially convective stars

N. R. Landin,^{1,2*} L. T. S. Mendes,^{3,2} L. P. R. Vaz² and S. H. P. Alencar²

¹Universidade Federal de Viçosa, Campus UFV Florestal, CEP 35690-000 – Florestal, MG, Brazil

²Depto. de Física, Universidade Federal de Minas Gerais, C.P.702, 31270-901 – Belo Horizonte, MG, Brazil

³Depto. de Engenharia Eletrônica, Universidade Federal de Minas Gerais, C.P.702, 31270-901 – Belo Horizonte, MG, Brazil

Accepted XXX. Received YYY; in original form ZZZ

ABSTRACT

We investigate stellar magnetic activity from the theoretical point of view, by using stellar evolution models to calculate theoretical convective turnover times (τ_c) and Rossby numbers (Ro) for pre-main-sequence and main-sequence stars. The problem is that the canonical place where τ_c is usually determined (half a mixing length above the base of the convective zone) fails for fully convective stars and there is no agreement on this in the literature. Our calculations were performed with the ATON stellar evolution code. We concentrated our analysis on fully and partially convective stars motivated by recent observations of slowly rotating fully convective stars, whose X-ray emissions correlate with their Rossby numbers in the same way as in solar-like stars, suggesting that the presence of a tachocline is not required for magnetic field generation. We investigate the behaviour of τ_c over the stellar radius for stars of different masses and ages. As Ro depends on τ_c , which varies strongly with the stellar radius, we use our theoretical results to determine a better radial position at which to calculate it for fully convective stars. Using our alternative locations, we fit a sample of 847 stars in the rotation-activity diagram (L_X/L_{bol} versus Ro) with a two-part power-law function. Our fit parameters are consistent with previous work, showing that stars with $\text{Ro} \leq \text{Ro}_{\text{sat}}$ are distributed around a saturation level in L_X/L_{bol} and, for stars with $\text{Ro} > \text{Ro}_{\text{sat}}$, L_X/L_{bol} clearly decays with Ro with an exponent of -2.4 ± 0.1 .

Key words: stellar evolution – stellar interiors – rotation – pre-main sequence – magnetic activity – convection

1 INTRODUCTION

Stars of different spectral types and ages host large-scale magnetic fields, as evidenced by observable phenomena like star spots, flares, activity cycles, coronal heating and chromospheric and coronal emissions, all of which express in some way stellar magnetic activity. Magnetic fields are observed in most (if not all) low-mass pre-main-sequence (pre-MS) and main-sequence (MS) stars (spectral types F, G, K and M, Donati & Landstreet 2009). However, only 5–10 per cent of intermediate mass stars (Herbig Ae/Be and A-B5 MS stars, VILLEBRUN et al. 2019 and Alecian et al. 2019) and 7% of high-mass MS stars (of spectral types O-B5, Keszthelyi et al. 2020) exhibit detectable magnetic fields.

From a theoretical point of view, a moving plasma subjected to a magnetic field is described by the magneto-hydrodynamic (MHD) equations and the dynamo theory is used as a main tool to investigate the processes responsible for keeping and regenerating stellar magnetic fields. The mechanism driving magnetic activity is generally attributed to a dynamo resulting from the interaction between differential rotation and convective motions in the outer convective envelope of the star. Theoretical results point out that, for MS solar type stars, the magnetic field is generated and amplified at the tachocline, a thin layer of differential rotation located at the interface between the internal radiative core and the external convective envelope. For stars of spectral types between F and M, magnetic activity and rotation are believed to be regulated by a dynamo process

called α - Ω effect (Mohanty & Basri 2003). In the Ω effect, differential rotation distorts the poloidal field in order to generate the toroidal field, while in the α effect, helical turbulence twists the toroidal field to regenerate the poloidal field. In this type of dynamo, the α and Ω effects are such that the poloidal and toroidal field components sustain themselves through a cyclic feedback process (Nelson 2008). The efficiency of this process depends on the rotation rate and on the convective motion time scale. Young, fast rotating stars are generally very active. Dynamo theory models, such as the α - Ω (or interface dynamo), have been successful in explaining qualitative features of solar magnetic activity (Weiss & Tobias 2000). For fully convective stars, such as very low-mass MS stars ($M < 0.35 M_{\odot}$) and very young stars in the pre-MS, this theory cannot be applied, because they are missing a tachocline. However, there are observations of magnetic activity indicators of fully convective stars and measurements of their magnetic field topology (Morin et al. 2010), some kind of dynamo should be in action in these stars. Durney et al. (1993) suggested that a distributed or turbulent dynamo could be operating in completely convective stars.

From the observational point of view, Kraft (1967), Frazier (1970) and Skumanich (1972) carried out pioneering works relating rotation to magnetic activity. Skumanich (1972) suggested for the first time that the rotation-activity relationship was a consequence of the dynamo action and showed that the stellar rotation rate decreases with age as $t^{-1/2}$. Pallavicini et al. (1981) showed that the fractional X-ray luminosity (L_X/L_{bol}) is correlated with the projected rotational velocity $v \sin i$ (and anti-correlated with rotation period). However, as pointed out by Noyes et al. (1984), the rotation-activity corre-

* E-mail: nlandin@ufv.br

lation is usually better described in terms of the Rossby number Ro , defined as the ratio of the rotational period P_{rot} to the local convective turnover time τ_c ($Ro = P_{\text{rot}}/\tau_c$). By analysing chromospheric activity indicators in stars of spectral types between F and M, [Soderblom et al. \(1993\)](#) verified that chromospheric magnetic activity increases rapidly with rotational velocity until $v \sin i \approx 15$ km/s, and then reaches a saturation plateau above this velocity threshold. Similar behaviours are also found with coronal magnetic activity indicators, as shown by, e.g., [Stauffer et al. \(1994\)](#). When analysed in terms of Rossby numbers, the saturation occurs for $Ro \lesssim 0.1$, which is equivalent to rotation periods of 1 to 10 d for solar-like stars. [Pizzolato et al. \(2003\)](#) extended the sample of [Noyes et al. \(1984\)](#) and showed the existence of two distinct regions: the saturated region (formed by fast rotators) and the unsaturated region (composed by slow rotators). [Prosser et al. \(1996\)](#) suggested the existence of a third regime, called supersaturation, which occurs for small values of Ro ($Ro < 0.01$). In this regime, also observed by [Randich et al. \(1996\)](#), stars with high rotation rates exhibit magnetic activity levels below the saturation level. According to [Argiroffi et al. \(2016\)](#), two physical mechanisms can be considered to explain this phenomena: centrifugal stripping¹ ([Jardine & Unruh 1999](#)) and polar updraft migration² ([Stepień et al. 2001](#)).

Magnetic activity indicators can be expressed as a function of Ro in the unsaturated region, but they are constant in the saturated regime. It characterises the rotation-activity relationship, which is a powerful tool in studies involving stellar dynamo processes, based on a general power-law function of the form $L_X/L_{\text{bol}} \propto Ro^\beta$ (using L_X/L_{bol} as an indicator of coronal activity), where β is a parameter to be adjusted with observations and canonically is -2 ([Pizzolato et al. 2003](#)). More recently, [Wright et al. \(2011\)](#), [Wright et al. \(2018\)](#) and [Newton et al. \(2017\)](#) analysed the rotation-activity relationship for samples of 824, 847 and 466 stars, respectively. The first two determined the level of the saturation regime in $L_X \approx 10^{-3} L_{\text{bol}}$ and power-law slopes of $\beta = -2.70 \pm 0.13$ ([Wright et al. 2011](#)) and $\beta = -2.3^{+0.4}_{-0.6}$ ([Wright et al. 2018](#)). [Newton et al. \(2017\)](#) found $\beta = -1.7 \pm 0.1$ and a saturation level of $L_{H_\alpha} \approx 10^{-4} L_{\text{bol}}$, where L_{H_α} (H_α luminosity) is a chromospheric activity indicator.

The Rossby number is an important parameter not only in stellar activity investigations, but also in astrophysical fluid dynamics (Ro is a measure of the importance of rotation in the fluid flow) and in MHD simulations. By describing the rotation-activity relationship in terms of the Rossby number, one can readily see its connection with stellar dynamo models. The reason for this, as pointed out by [Kim & Demarque \(1996\)](#), is that the dynamo number N_D , a dimensionless parameter in the mean-field dynamo theory which characterises the model behaviour, is proportional to the inverse square of Rossby number. By its turn, the dynamo number is essentially the ratio between the terms of magnetic field generation and diffusion. As long as $N_D \propto Ro^{-2}$, the dynamo efficiency, and consequently the level of magnetic activity, increases with decreasing Rossby number. As Ro plays an important role in the stellar magnetic activity studies, determinations of τ_c are of fundamental interest, because they cannot be directly observed. Unfortunately, our limited knowledge of stellar convection imposes a strong challenge for correct convective turnover time calculations. Even when we rely on the Mix-

ing Length Theory approximation, extensively used in the literature, some uncertainties are still involved. For instance, the assumption of the same mixing length parameter α for modelling stars of different masses and evolutionary stages ([Kim & Demarque 1996](#)).

Though τ_c can only be assessed theoretically with stellar models, it has been customary in the literature to employ its semi-empirical value, a theoretically derived τ_c expressed as function of an observed colour index. In their works concerning the rotation-activity relation, [Noyes et al. \(1984\)](#) and [Pizzolato et al. \(2003\)](#) used $\tau_c(B-V)$, [Wright et al. \(2018\)](#) utilised $\tau_c(V-K)$ and [Wright et al. \(2011\)](#) handle with both semi-empirical colour functions of τ_c . Among the published estimates of τ_c which come from models that track the stellar evolution, we describe four in more detail. [Gilliland \(1986\)](#) did theoretical estimates of convective turnover times by using simple standard models described by [Eggleton \(1971, 1972\)](#). [Kim & Demarque \(1996\)](#) published convective turnover times for solar-like stars in the pre-MS and early post-main-sequence phases of evolution. They used non-grey boundary conditions, but the opacities used in their work are less up-to-date than those we use. [Jung & Kim \(2007\)](#) presented convective turnover times for low- and very low-mass stars in the pre-MS. Although they published a finer grid resolution than we do, their models did not take into account stellar rotation and used grey boundary conditions, which are not suitable for effective temperatures below about 4000K ([Baraffe et al. 1997](#)). [Landin et al. \(2010\)](#) computed convective turnover times for rotating, grey models ranging from 0.6 to 1.2 M_\odot with solar chemical composition.

The rotation-activity relationship (magnetic activity increasing with decreasing Rossby number down to $Ro \approx 0.1$ and remaining constant for $Ro \leq 0.1$), clearly observed for MS stars, cannot be seen among pre-MS stars (e.g. [Flaccomio et al. 2003](#) and [Feigelson et al. 2003](#)). In this evolutionary phase, all stars are found to be in the saturated regime and a considerable dispersion in the magnetic activity levels is observed, as [Preibisch et al. \(2005\)](#), [Alexander & Preibisch \(2012\)](#) and [Argiroffi et al. \(2014\)](#) have shown for stars in Orion Nebula Cluster (1 Myr), IC348 (2-3 Myr) and h Per (13 Myr), respectively. Until recently, it was believed that the saturated part of the rotation-activity relationship was composed by partially and totally convective stars with high rotation rates while the unsaturated part was formed only by partially convective stars with slow rotation rates. However, recent observations by [Wright & Drake \(2016\)](#) and [Wright et al. \(2018\)](#) of X-ray emission of slowly rotating fully convective stars indicate that partially and fully convective stars follow the same rotation-activity relationship. According to [Wright & Drake \(2016\)](#), as this relationship is considered a proxy for the behaviour of the magnetic dynamo, these results imply that partially and fully convective stars should operate very similar rotation-dependent dynamos. Because standard dynamo model is based on the shearing of internal magnetic fields by differential rotation that takes place at the tachocline, which is not present in fully convective stars, the results of [Wright & Drake \(2016\)](#) and [Wright et al. \(2018\)](#) imply that the presence of a tachocline is not a central key for magnetic field generation. In these cases, as they also mentioned, there are other possibilities for large-scale magnetic field generation such as the turbulent or the distributed dynamos (see e.g. [Brun & Browning 2017](#), for a review on this subject).

In order to contribute to a better understanding of the dynamo mechanism existing in fully and partially convective stars, we study the behaviour of the parameters related to Rossby numbers inside stars of different masses and ages with the ATON stellar evolution code. For a given stellar mass and age, the convective turnover time changes significantly depending on the location inside the star at which it is calculated. The location mostly used in the literature to

¹ A predicted reduction of the coronal emission at high rotational velocities, due to the disruption of the largest coronal structures by centrifugal forces.

² Polar updraft migration is that, at high rotational velocities, the magnetic flux emergence becomes more efficient near the poles, diminishing or even vanishing magnetic flux tubes and coronal structures at equatorial regions.

determine τ_c is near the base of the convective zone, one mixing length (Gilman 1980) or one half a mixing length (Noyes et al. 1984) above it. This choice is based on the assumption that the source region of the stellar magnetic dynamo matches that of the tachocline (Parker 1975). Observational results showing that the intensity of the chromospheric emission (H & K lines of Ca II) of solar-type stars and Rossby number calculated at one half a mixing length above the base of the convective zone correlate well (Schatzman et al. 1993), seem to support it. However, these locations are not suitable for fully convective stars, including young pre-MS stars and MS very low-mass stars.

Section 2 briefly presents the physical ingredients of the ATON code and the input parameters used in this work. Section 3 presents our theoretical convective turnover times and convective velocities. Aiming at finding an alternative location to calculate τ_c for young stars and very low-mass stars, but still related to the default location, we evaluate τ_c throughout the whole star, investigate its behaviour for different stellar masses and ages, analyse where it is usually calculated for masses greater than $0.4 M_\odot$ (mass interval in which all stars are partially convective in the MS), and propose an alternative location to calculate it for fully convective stars. Section 4 discusses results on local convective turnover times and Rossby number calculations. In Section 5, our new theoretical convective turnover times are compared with those available in the literature and observational data from low-mass and very-low mass stars are used to test our theoretical results. Finally, our conclusions are given in Section 6.

2 MODELS AND INPUT PHYSICS

In the ATON code version used in this work, convection is treated according to the traditional Mixing Length Theory (Böhm-Vitense 1958), with the parameter that represents the convection efficiency $\alpha=2$. Surface boundary conditions were obtained from non-grey atmosphere models (Allard et al. 2000) with matching between the surface and interior at optical depth $\tau=3$. We used the opacities reported by Iglesias & Rogers (1993) and Alexander & Ferguson (1994) and the equations of state from Rogers et al. (1996) and Mihalas et al. (1988). Here, we assume that the elements are mixed instantaneously in convective regions. Our tracks start from a fully convective configuration with central temperatures in the range $5.35 < \log_{10} T_c < 5.72$, follow deuterium and lithium burning, and end at the MS configuration. For a discussion about the zero point of ages of stellar models see Landin et al. (2006).

The current version of the ATON code allows choosing among three rotational schemes (Mendes et al. 1999), (1) rigid body rotation throughout the whole star, (2) local conservation of angular momentum in the whole star (which leads to differential rotation) and (3) local conservation of angular momentum in radiative regions plus rigid body rotation in convective regions. However, there is observational evidence that the Sun's radiative core rotates as a solid body and the convective envelope rotates differentially, opposite to scheme 3 (Thompson et al. 2003). Here, our rotating models were generated according to scheme 2 because differential rotation in the convective envelope is an important ingredient to the dynamo process. We leave for the future implementation of a 4^{th} rotational scheme with a rotational profile closer to that of the Sun.

The initial angular momentum of each model is obtained according to Kawaler (1987) as

$$J_{\text{kaw}} = 1.566 \times 10^{50} \left(\frac{M}{M_\odot} \right)^{0.985} \text{ g cm}^2 \text{ s}^{-1}. \quad (1)$$

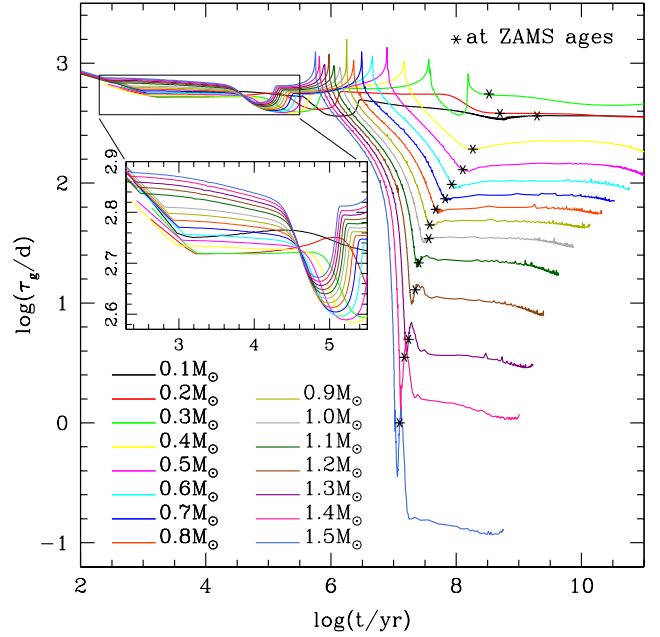


Figure 1. Global convective turnover time as a function of age t and stellar mass. Asterisks (*) show the ZAMS ages for each mass model. The insert shows in detail the temporal evolution of τ_g during the beginning of the pre-MS phase. Throughout this work all the logarithms are taken in base 10.

The evolutionary tracks were computed in the mass range of 0.1 to $1.5 M_\odot$ (in $0.1 M_\odot$ steps). We adopt the solar chemical composition $X=0.7155$ and $Z=0.0142$, by Asplund et al. (2009). More details on the physics of the ATON models are given by Landin et al. (2006).

3 CONVECTIVE TURNOVER TIMES CALCULATIONS

There are two ways to calculate theoretical convective turnover times using stellar evolution models, locally and non-locally. This section presents the details of such calculations in the ATON code. We also investigate how convective turnover times and convective velocities vary with stellar mass and age. For some selected ages, we examine the behaviour of radial profiles of these quantities for stellar masses from 0.1 to $1.5 M_\odot$, aiming to find an alternative location to calculate convective turnover times locally.

3.1 Global convective turnover times

Following Kim & Demarque (1996), we evaluate the global (or non-local) convective turnover time (τ_g) for each model (see Fig. 1). The global convective turnover time is defined as $\tau_g = \int_{R_b}^{R_{\text{star}}} v_c^{-1} dr$, where R_b is the radial position of the base of the convective zone relative to the centre of the star, R_{star} is the stellar radius and v_c is the convective velocity. According to Kim & Demarque (1996), this is the characteristic time-scale for convective overturn. It can be used to describe convection features of the whole stellar convective region at each evolutionary stage. We note that in Fig. 1 the time evolution of τ_g differs for fully and partially convective stars. Global convective turnover times of very low-mass stars ($M \leq 0.3 M_\odot$) present small variations (less than 0.6 dex – a factor of 3.5), while for stars with $M > 0.3 M_\odot$ variations in τ_g can reach almost 4 orders of magnitude. Values of τ_g do not change significantly near the beginning of the

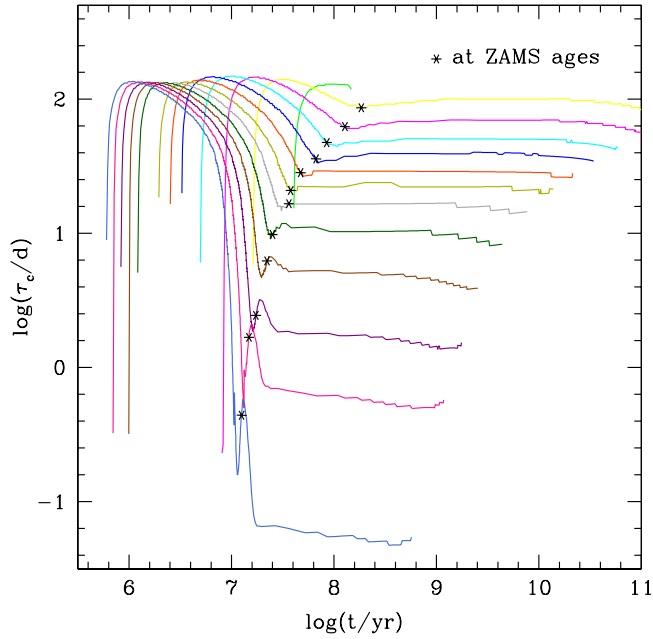


Figure 2. Local convective turnover time as a function of age and stellar mass. Symbols and colours have the same meanings as in Fig. 1. The calculations were performed only while $r_{\text{std}} < R_{\text{star}}$, where r_{std} , our standard location to calculate τ_c , is defined as one-half of a mixing length above the base of the convective zone.

pre-MS phase, in which stars are fully convective, decrease when stars develop a radiative core and remain roughly constant during the MS phase. For $M > 1.3 M_{\odot}$, τ_g experiences an extra reduction after the zero-age main sequence (ZAMS, asterisks in Fig. 1) and before reaching its nearly constant MS value. It reflects the behaviour of the pressure scale-height for such models. During the pre-MS, the higher the stellar mass the higher τ_g , except for $M \leq 0.3 M_{\odot}$, when the opposite situation is observed (see the amplified view in Fig. 1). On the MS, τ_g decreases as the mass increases for $M > 0.3 M_{\odot}$ but for $M \leq 0.3 M_{\odot}$ τ_g increases with mass.

3.2 Local convective turnover times

For the purpose of computing Rossby numbers, the characteristic time-scale used is the local convective turnover time, calculated in the deep convection envelope where dynamo generation of magnetic fields is supposed to take place. The local convective turnover time is defined as the ratio of convection mixing length (ℓ) to convective velocity, $\tau_c = \ell/v_c$. Following Noyes et al. (1984), we adopt as the standard location (r_{std}) to calculate τ_c at one-half of a mixing length above the base of the convective zone $r_{\text{std}} = R_b + \ell/2$, where ℓ is evaluated at the base of the convective zone. In Fig. 2, we show local convective turnover times calculated at the standard location as a function of age, for some stellar models. Local convective turnover times vary significantly with age before the ZAMS and remain virtually constant during the MS. On the MS τ_c decreases with the stellar mass. One can notice in Fig. 2 that the $0.3 M_{\odot}$ model (green curve) seems to be incomplete and the 0.1 and $0.2 M_{\odot}$ models (black and red curves, respectively) are not shown. The reason is that, for fully convective stars, the base of the convective zone is the stellar centre, which is singular (Gilliland 1986). Besides $M(r) = 0$ and $L(r) = 0$ at the stellar centre, in Mixing Length Theory, the adjustable parameter, the mixing length, is scaled with the local pressure scale

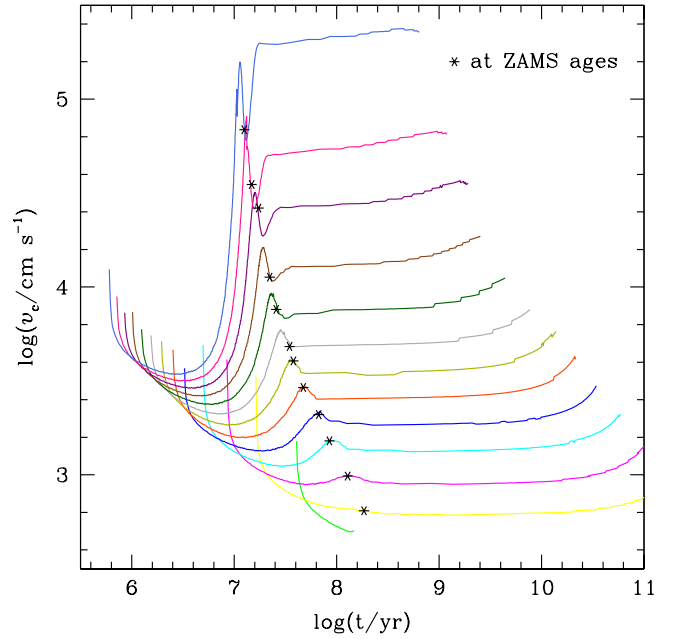


Figure 3. Convective velocity as a function of age and stellar mass. Symbols and colours have the same meanings as in Fig. 1. The calculations were performed only while $r_{\text{std}} < R_{\text{star}}$.

height H_p through the relation $\ell = \alpha H_p$ and, for these models, H_p at the base of the convective zone is very high, and so is the mixing length. Consequently, the place where τ_c should be calculated, $r_{\text{std}} = R_b + \alpha H_p/2$, becomes larger than the stellar radius. As r_{std} depends on the adjustable parameter α , one could think of using an alternative α_{alt} whenever $r_{\text{std}} > R_{\text{star}}$. However, to accomplish this, α_{alt} should be smaller than 0.02, at least two orders of magnitude smaller than that which reproduces the Sun, implying a very inefficient convective energy transport. So, these facts reinforce the idea that applying prescriptions based explicitly on the tachocline to obtain the place where the magnetic field is produced and amplified in fully convective stars is senseless (Feiden 2013). For all the reasons discussed above, we believe that the usual location in the stellar interior used to calculate Ro is not suitable for fully convective stars. In cases which $r_{\text{std}} > R_{\text{star}}$, τ_c is not calculated.

3.3 Convective velocities

Both τ_c and τ_g represent characteristic time scales for stellar convection and so should differ only by a constant factor. Because these two quantities depend on the convective velocity, we show how this behaves as function of stellar age and mass in Fig. 3, again only for ages and masses for which τ_c can be calculated at the standard location. Before reaching the ZAMS (marked with asterisks), v_c varies significantly with stellar age but remains roughly constant on the MS. For models with $M > 1.3 M_{\odot}$, v_c is subjected to an extra variation before becoming approximately constant on the MS. This is due to variations in the pressure scale-height occurring in such models. In this phase, the convective velocity increases with the stellar mass.

3.4 Radial profiles of Ro, τ_c and v_c at the ZAMS

In order to set an alternative location to calculate the local convective turnover time for fully convective stars during the MS and pre-MS

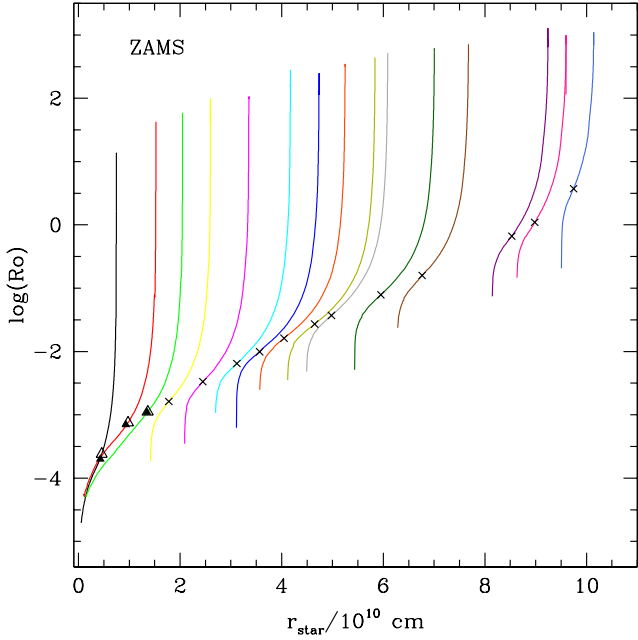


Figure 4. Rossby number Ro as a function of radius r_{star} through the star for each mass model. Crosses (\times) show the standard locations inside the stars where τ_c is usually calculated (for $M \geq 0.4 M_{\odot}$). Colours are as in Fig. 1 and triangles (\blacktriangle , \triangle) are explained in the main text, Section 3.5.

phases, we investigate the stellar interior properties related to this quantity, evaluating the Rossby number, the convective velocity and the local convective turnover time itself throughout the whole star. First, we analyse how Rossby numbers vary inside the stars for all models at the ZAMS. From Fig. 4, we can see that the Rossby number profiles seem to be very steep, when plotted on a length scale covering several times the extensions of their corresponding convective zones. Actually, these profiles have steep inclinations only near the stellar centre and the stellar surface, being considerably less steep at intermediate stellar radii. Here, Ro was obtained with τ_c and P_{rot} of each radial shell of the star. Because our models include differential rotation, P_{rot} varies with the distance relative to the star’s centre. In this plot, we identify with crosses the standard location inside the stars where τ_c is usually calculated. We note that, for each model, this coincides with the less steep region of the Ro radial profile.

The behaviour of Ro with radius at the ZAMS, shown in Fig. 4, depends on the convective turnover time profiles (Fig. 5) which, in turn, depend on convective velocity profiles, shown in Fig. 6. Both curves also vary steeply when plotted on large length scales and r_{std} localises around the less steep regions of the profiles, similar to Ro .

3.5 Parameterisations of r_{std} at the ZAMS

Continuing our effort to find an alternative place to calculate τ_c inside fully convective stars, we next express the standard location in terms of other quantities, such as the stellar radius R_{star} and the pressure scale height H_p . In Fig. 7, we show these standard locations as a function of age and mass for models with $M \geq 0.4 M_{\odot}$.

The standard location r_{std} varies from about 0.65 to 0.95 R_{star} in the mass range of 0.4 to 1.5 M_{\odot} at the ZAMS. Black squares (\blacksquare) indicate r_{std} inside the stars at the ZAMS. We analysed how $r_{\text{std}}/R_{\text{star}}$ varies as a function the stellar mass and found that it behaves ap-

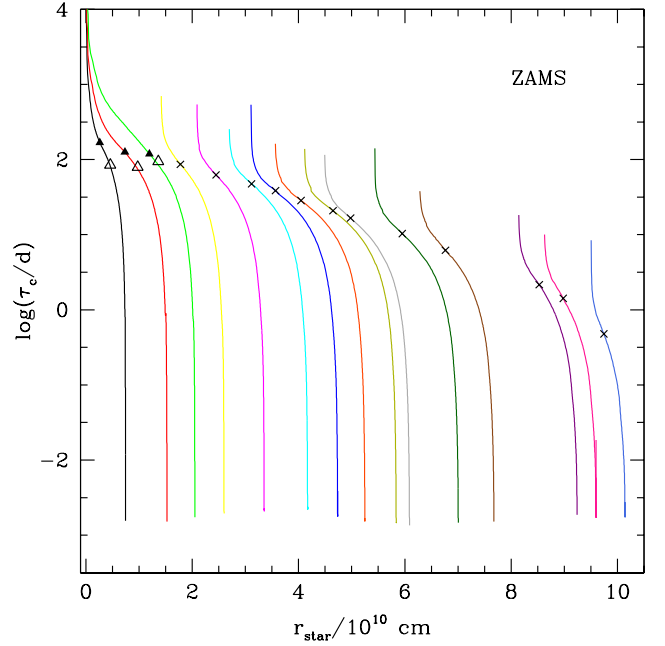


Figure 5. Local convective turnover time τ_c versus radius r_{star} for each stellar model. Symbols are as in Fig. 4 and colours are as in Fig. 1.

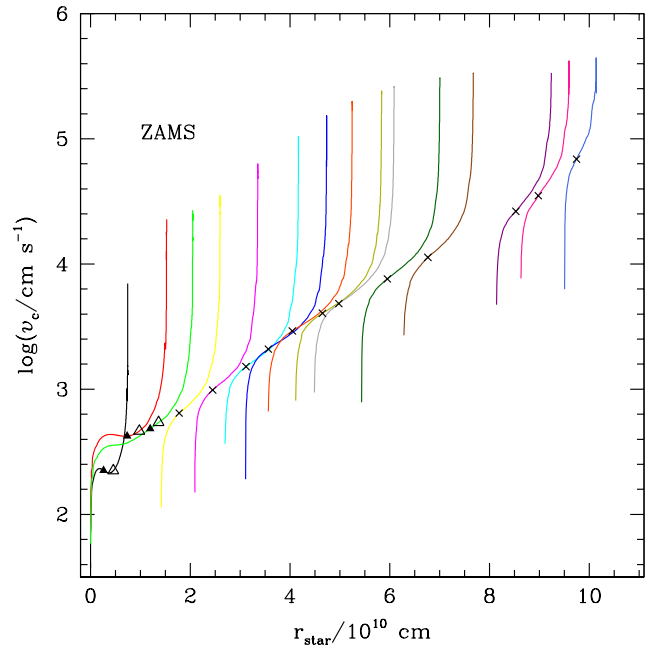


Figure 6. Convective velocity v_c versus the stellar radius r_{star} for each mass model. Symbols are as in Fig. 4 and colours as in Fig. 1.

proximately linearly. We then made a linear fit to the data obtaining $r_{\text{std}}/R_{\text{star}} = (0.25 \pm 0.01)M/M_{\odot} + (0.59 \pm 0.01)$. Through an extrapolation of this fit to the lower mass regime, we estimate that the local convective turnover time can be calculated as 0.615, 0.640 and 0.665 R_{star} respectively for 0.1, 0.2 and 0.3 M_{\odot} above the base of the convective zone at the ZAMS. These extrapolations are shown in Fig. 7 as open squares (\square). Aiming to visualise where our predicted positions to calculate τ_c at the ZAMS for 0.1, 0.2 and 0.3 M_{\odot} would be located relative to the Ro , τ_c and v_c profiles, we marked

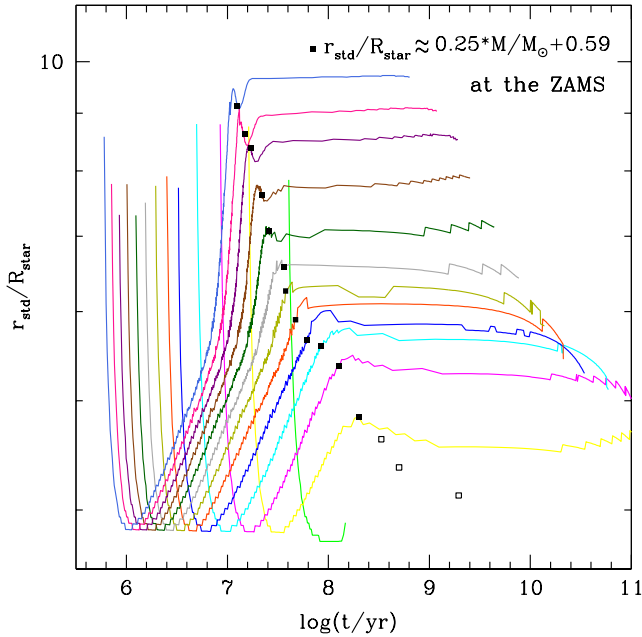


Figure 7. The standard location where τ_c is calculated in units of stellar radius versus age t for each stellar model. Filled squares (■) represent these locations at the ZAMS for $M \geq 0.4 M_\odot$. Open squares (□) represent extrapolations to 0.1, 0.2 and $0.3 M_\odot$. Colours are as in Fig. 1.

them, respectively in Figs 4, 5 and 6 with black open triangles (Δ). The trends followed by our predicted positions in the Ro and v_c profiles are similar to those corresponding to the locations of r_{std} for $M \geq 0.4 M_\odot$ (crosses - \times). However, for the τ_c profile this behaviour is not seen and results in predicted positions that are below expectations and that do not change significantly with mass in the range of $0.1 \leq M/M_\odot \leq 0.3$.

Repeating this procedure for H_p we show, in Fig. 8, the standard locations where τ_c should be calculated in terms of H_p as a function of age and mass for models with $M \geq 0.4 M_\odot$. Black squares (■) indicate r_{std} inside the stars at the ZAMS. We note that r_{std} lies in the interval of 7 to 70 H_p in the mass range of 0.4 to $1.5 M_\odot$ at the ZAMS. The variation of r_{std}/H_p with mass deviates more from a linear behaviour than does $r_{\text{std}}/R_{\text{star}}$, mainly for $M > 1.0 M_\odot$. For this reason, we performed a linear fit with r_{std}/H_p and M for $M \leq 1.0 M_\odot$ finding $r_{\text{std}}/R_{\text{star}} = (10.4 \pm 0.9)M/M_\odot + (3.4 \pm 0.7)$. An extrapolation of this fit to lower masses indicates that the local convective turnover time should be calculated at 4.44, 5.48 and 6.53 H_p , respectively for 0.1, 0.2 and $0.3 M_\odot$ above the base of the convective zone at the ZAMS. These extrapolations are shown in Fig. 8 as open squares (□) and their corresponding locations relative to the Ro, τ_c and v_c profiles in Figs 4, 5 and 6 respectively are marked with black filled triangles (\blacktriangle). In these latter Figures, we can see that our predicted positions in the Ro, τ_c and v_c profiles follow the same trends as the corresponding locations of r_{std} values for $M \geq 0.4 M_\odot$ (crosses - \times). Our extrapolated positions to calculate τ_c were compared to those predicted by Feiden (2013). He used results of full 3D MHD models of fully convective stars ($0.3 M_\odot$) obtained by Browning (2008). These suggest that the magnetic field strength is maximum at about $0.15 R_{\text{star}}$, and Feiden (2013) assumed that this radial position plays the same role as the tachocline in partly convective stars. So, he calculated the Rossby number at one half of a mixing length above $0.15 R_{\text{star}}$. In order to make this comparison, we used the values of R_{star} and ℓ yielded by the ATON code for each stellar mass. Both lo-

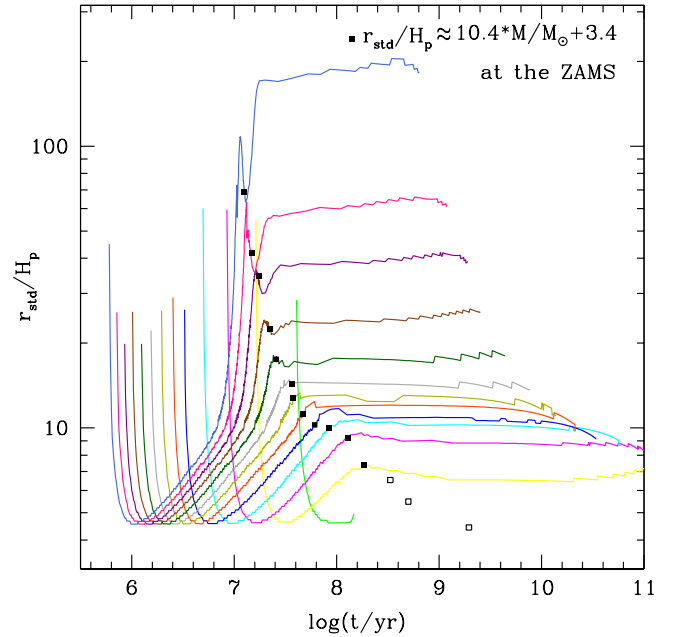


Figure 8. The standard location where τ_c is calculated in units of H_p versus the stellar age t for some models. Symbols are as in Fig. 7 and colours are as in Fig. 1.

cations are, to a certain degree, consistent with each other, because they are found in the less steep region of the Ro, τ_c and v_c profiles; our predicted positions are about 10% smaller than those of Feiden (2013) but the places where our tachocline-like region should be are 0.37 , 0.45 and $0.51 R_{\text{star}}$, respectively for 0.1, 0.2 and $0.3 M_\odot$.

We next investigate the stellar interior near the point where τ_c should be calculated (both standard and predicted positions) aiming to find some correlations with the stellar properties. In Fig. 5, we note that the standard positions (defined for $M \geq 0.4 M_\odot$) and our predicted positions (defined for $M < 0.4 M_\odot$) are found near the inflection point of the curves, as was confirmed by 2nd derivative calculations of 3rd degree spline fits. In order to have a better comprehension of this coincidence it would be useful to inspect results of MHD simulations, which can provide us important informations about the dynamo process in such regions.

As can be seen in Fig. 7, $r_{\text{std}}/R_{\text{star}}$ does not vary significantly after the ZAMS. From Fig. 8, the same behaviour is found for r_{std}/H_p for $M \leq 1.3 M_\odot$ but for larger masses the roughly constant MS r_{std}/H_p are higher than the corresponding ZAMS. At first, this could indicate that the $r_{\text{std}}/R_{\text{star}}$ scaling should be favoured over the r_{std}/H_p scaling to estimate the location where τ_c should be calculated but on the other hand, it underestimates such positions for stars in the most critical mass regime of our analysis ($M \leq 0.3 M_\odot$, in which stars are fully convective throughout their entire evolution). Taking this fact into account, hereinafter we will adopt the description of r_{std} in terms of H_p .

Then, we used our r_{std}/H_p linear fit as a function of mass at the ZAMS to estimate τ_c for the 4 slowly rotating fully convective stars in the sample of Wright & Drake (2016), the first to be found in the unsaturated region of the activity-rotation diagram. Fig. 9 illustrates this, showing L_X/L_{bol} versus Ro for 828 stars. Among them 824 are from the sample of Wright et al. (2011), which is composed by partially convective stars (\circ) and fast rotating fully convective stars (\bullet). Fig. 9 also shows the 4 slowly rotating fully convective stars

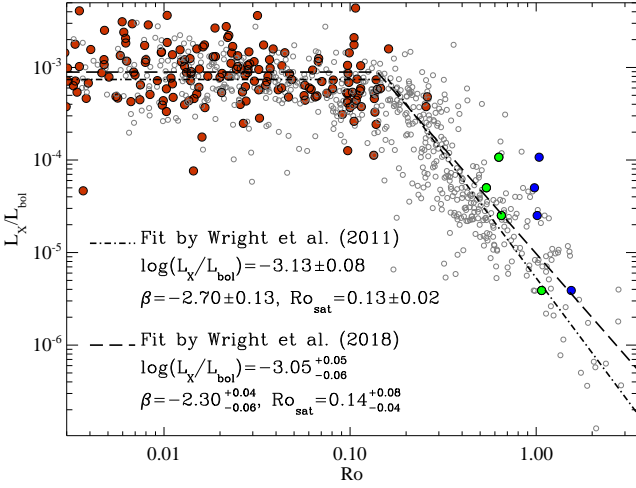


Figure 9. Fractional X-ray luminosity as a function of the Rossby number for 828 stars in the samples of Wright et al. (2011) and Wright & Drake (2016). Fast rotating fully convective stars are shown as filled dark red circles (●) and partially convective stars as grey open circles (○). The four slowly rotating fully convective stars are shown with Ro calculated with two different τ_c values, semi-empirically (filled green circles, ●) or theoretically according to this work (filled blue circles, ●). The dash-dotted and long-dashed lines show the best-fitting activity-rotation relationships found by Wright et al. (2011) and Wright et al. (2018), respectively.

(●) from the sample of Wright & Drake (2016). The dash-dotted line is the best fit found by Wright et al. (2011) for the 824 stars in their sample and the long dashed line is the best fit found by Wright et al. (2018) for these 824 stars plus 23 slow rotating fully convective stars. Wright et al. (2011) and Wright & Drake (2016) used the semi-empirical determinations of local convective turnover times of Pizzolato et al. (2003) to calculate the Rossby number of their sample of stars. In order to test our preliminary results, we calculated the Rossby numbers of these 4 fully convective stars, in the sample of Wright & Drake (2016), using our theoretical τ_c . Their positions in the rotation-activity diagram obtained with our τ_c are shown in blue filled circles (●) in Fig. 9. Though our Ro are slightly higher about 1.5 times) than those of Wright & Drake (2016), they still keep the corresponding stars in the unsaturated region.

3.6 Parameterisations of r_{std} at different ages

After achieving promising results with the previous fit and τ_c estimate, we repeated the procedure described in Section 3.5 for some stellar ages t , namely, $\log(t/\text{yr}) \in \{6.0, 6.5, 7.0, 7.5, 8.0, 8.5, 9.0, 9.5, 10.0, 10.14\}$. For each of these ages, we performed a linear fit to r_{std}/H_p as a function of the stellar mass. Table 1 shows details of each linear fit for a given age. For $\log(t/\text{yr}) \leq 6.0$, we used the fit obtained for $\log(t/\text{yr}) = 6.0$ to find the location to calculate τ_c . For ages in the interval of $6.0 < \log(t/\text{yr}) \leq 6.5$, we interpolate r_{std}/H_p with the fits obtained for $\log(t/\text{yr}) = 6.0$ and $\log(t/\text{yr}) = 6.5$. For ages in the interval of $6.5 < \log(t/\text{yr}) \leq 7.0$, we made a similar interpolation but with fits found at $\log(t/\text{yr}) = 6.5$ and $\log(t/\text{yr}) = 7.0$. The next intervals were divided in the same way, every 0.5 dex, except the last one, for which the interpolation was done with the fits obtained at $\log(t/\text{yr}) = 10.0$ and $\log(t/\text{yr}) = 10.14$. The mass interval used in our linear fits differs for each age. The minimum mass in each mass range is $0.4 M_\odot$, except in cases in which the models have large mixing lengths placing r_{std} outside the stars. This happens

Table 1. Details of linear fits with the equation $r_{\text{std}}/H_p = AM/M_\odot + B$. Column 1 gives the logarithm of stellar age; col. 2 the mass range used in the fit of r_{std}/H_p ; col. 3 the coefficient A; and col. 4 the coefficient B.

$\log(t/\text{yr})$	Mass range M_\odot	coefficient A	coefficient B
6.00	1.3 to 1.5	-6 ± 2	14 ± 3
6.50	0.9 to 1.5	3.6 ± 0.3	1.1 ± 0.3
7.00	0.6 to 1.2	7.2 ± 0.3	0.0 ± 0.3
7.50	0.4 to 0.9	13 ± 1	7.2 ± 0.8
8.00	0.4 to 1.2	18 ± 3	-1 ± 2
8.50	0.4 to 1.2	17 ± 3	-1 ± 2
9.00	0.4 to 1.1	14 ± 1	1 ± 1
9.50	0.4 to 1.1	13 ± 2	1 ± 1
10.00	0.4 to 1.0	8 ± 2	4 ± 1
10.14	0.4 to 0.9	9 ± 2	4 ± 1
ZAMS	0.4 to 1.0	10.4 ± 0.9	3.4 ± 0.7

for $\log(t/\text{yr}) = 6.0$ below $1.3 M_\odot$, $\log(t/\text{yr}) = 6.5$ below $0.9 M_\odot$ and $\log(t/\text{yr}) = 7.0$ below $0.6 M_\odot$. Because the relations between r_{std}/H_p and M deviate more from a linear behaviour when more massive stars are included, some stellar masses were excluded from the fits. The exceptions are $\log(t/\text{yr}) = 10.0$, and $\log(t/\text{yr}) = 10.14$, for which stars with masses larger than $1.0 M_\odot$ and $0.9 M_\odot$, respectively, have already left the MS phase.

We analysed the radial profiles of τ_c and v_c for all selected ages in Table 1. Their behaviours are similar to those seen for these quantities at the ZAMS (Figs. 5 and 6). The predicted positions where τ_c should be calculated for models with $M < 0.4 M_\odot$, which are outside the interpolations intervals shown in Table 1, follow the same trend as the corresponding positions of r_{std} . They are found to be near the place where the curves are less steep. Because the fit for $\log(t/\text{yr}) = 6.0$ was made with the smallest number of points, it is the one with the largest departure from this trend. The radial τ_c profiles for $\log(t/\text{yr}) = 7.0$ present the same behaviour found as at the ZAMS, that the standard positions lie very close to the inflection point of the curves, as do our predicted positions. This was confirmed by calculations with 3rd degree spline fits. The analysis of the radial τ_c profiles is postponed to future work, when we will try to interpret our findings in the light of MHD simulation results.

4 RESULTS

The results obtained in Section 3 through linear fits of r_{std}/H_p as a function of mass were introduced in the ATON code as alternative locations to calculate τ_c for stars where $r_{\text{std}} > R_{\text{star}}$, for fully convective stars. Then, the evolution of local convective turnover times during the pre-MS and at the beginning of the MS was followed for 0.1 to $1.5 M_\odot$ stars and tabulated together with the corresponding evolutionary tracks. Table 2 presents the $1 M_\odot$ model as an example of such tables. Rotation periods are those evaluated by models for the surface layers, starting from the initial periods, which correspond to the initial angular momenta given in Eq. 1, and then evolving by considering conservation of angular momentum. In our models, we did not take into account angular momentum loss by stellar winds. This is the main reason why our $1 M_\odot$ model at the solar age shows a rotation period quite different from the current Sun. In order to reproduce it, we should have used the rotational scheme 3, described in Section 2, but we chose scheme 2 because differential rotation and its interaction with convection is the base of the solar dynamo model. To have an idea of how the choice of rotational scheme affects convective turnover time, we compared τ_c for $1 M_\odot$ at the Sun's age

Table 2. Evolutionary tracks, including τ_c , τ_g , P_{rot} and Ro , for a $1 M_{\odot}$ star^a. Column 1 gives the logarithm of stellar age; col. 2 the logarithm of bolometric luminosity; col. 3 the logarithm of effective temperature; col. 4 the logarithm of effective gravity; col. 5 the logarithm of local convective turnover times; col. 6 the logarithm of global convective turnover times; col. 7 the rotation period; and col. 8 the Rossby number.

$\log(t/\text{yr})$	$\log \frac{L}{L_{\odot}}$	$\log (T_{\text{eff}}/\text{K})$	$\log (g/\text{cm s}^{-2})$	$\log (\tau_c/\text{d})$	$\log (\tau_g/\text{d})$	P_{rot}/d	Ro
2.6848	1.6882	3.6059	2.126	1.9444	2.8296	185.776	2.1113
3.8668	1.5802	3.6337	2.345	1.9110	2.7955	103.295	1.2680
4.3506	1.3600	3.6441	2.607	1.9006	2.7781	58.140	0.7309
4.8159	1.1448	3.6526	2.856	1.8853	2.6430	33.698	0.4388
5.2182	0.9844	3.6574	3.036	1.8858	2.7335	22.858	0.2973
5.3960	0.8181	3.6611	3.217	1.8821	2.7695	14.976	0.1965
5.6561	0.5970	3.6633	3.447	1.8819	2.7758	8.929	0.1172
5.9360	0.3761	3.6617	3.661	1.8865	2.8091	5.498	0.0714
6.2263	0.1553	3.6572	3.864	1.8909	2.7400	3.477	0.0447
6.5282	-0.0652	3.6506	4.058	2.1183	2.5221	2.129	0.0162
6.8479	-0.2581	3.6476	4.239	2.0075	2.3410	1.405	0.0138
7.1062	-0.2979	3.6659	4.352	1.8314	2.1384	1.037	0.0153
7.2812	-0.1742	3.7077	4.396	1.6152	1.9158	0.880	0.0214
7.3982	-0.0095	3.7492	4.397	1.3542	1.6664	0.845	0.0374
7.5163	-0.0708	3.7640	4.517	1.2124	1.5173	0.648	0.0397
9.0239	-0.0894	3.7605	4.522	1.2321	1.5315	0.659	0.0386
9.4180	-0.0408	3.7644	4.489	1.2148	1.5253	0.704	0.0429
9.5787	0.0011	3.7674	4.459	1.1977	1.5018	0.747	0.0474
9.6992	0.0445	3.7699	4.425	1.1819	1.4831	0.804	0.0529
9.8050	0.1019	3.7723	4.378	1.1707	1.4858	0.888	0.0599

^aThe complete version of the table, including 15 tracks for masses in the range $0.1\text{--}1.5 M_{\odot}$ (in $0.1 M_{\odot}$ increments), will be available in electronic form at CDS via anonymous ftp to cdsarc.u-strasbg.fr (130.79.128.5) or via <https://cdsarc.uistra.fr/viz-bin/cat/J/MNRAS>. Remind that in this work all the logarithms are taken in base 10.

generated by models considering differential rotation throughout the whole star (scheme 2) and models considering differential rotation in the radiative core and rigid body rotation in the convective envelope (scheme 3) plus angular momentum loss by stellar winds. The difference between them was 5%.

According to our $1 M_{\odot}$ model at the age of the Sun, the solar local convective turnover time is $\tau_{c,\odot}=15.40$ d which corresponds to $\text{Ro}_{\odot}=1.69$ with $P_{\text{rot},\odot}=26.09$ d (Donahue et al. 1996). This value is consistent to that found semi-empirically by Pizzolato et al. (2003), which is $\tau_{c,\odot}=12.59$ d ($\text{Ro}_{\odot}=2.07$).

Fig. 10, similarly to Fig. 2, shows local convective turnover times as a function of age and mass. The ZAMS age of each mass model is shown with an asterisk. Compared to Fig. 2, Fig. 10 is extended, including τ_c calculations where $r_{\text{std}} > R_{\text{star}}$, for $M < 0.4 M_{\odot}$ (pre-MS and MS) and for the early pre-MS of stars with $M \geq 0.4 M_{\odot}$. With regard to the last case, the age at which r_{std} becomes smaller than R_{star} decreases as the mass increases, as expected from the stellar interior theory. For the $0.4 M_{\odot}$ model it is about $\log(t/\text{yr})=7.0$, while for the $1.5 M_{\odot}$ model it is about $\log(t/\text{yr})=6.0$. For models whose $r_{\text{std}} < R_{\text{star}}$, τ_c was calculated at one-half of a mixing length above the base of the convective zone. Otherwise τ_c was calculated at the alternative place, related to H_p . As explained in Section 3, for $\log(t/\text{yr}) \leq 6.0$ we use the same r_{std}/H_p linear fit found at $\log(t/\text{yr})=6.0$. This is why τ_c is approximately constant in this age range. For $\log(t/\text{yr}) \leq 6.0$ and $M \geq 0.4 M_{\odot}$, the larger the stellar mass the larger τ_c , while for $M < 0.4 M_{\odot}$ we cannot observe a regular behaviour (see the amplified view in Fig. 10). For $\log(t/\text{yr}) \geq 7.0$, τ_c increases as the stellar mass decreases, except for the mass range 0.1 to $0.4 M_{\odot}$ and $\log(t/\text{yr}) \gtrsim 9.3$. We believe that this irregular behaviour of models with $M < 0.4 M_{\odot}$ is probably a consequence of the method we used to determine where τ_c should be calculated. This was based on lin-

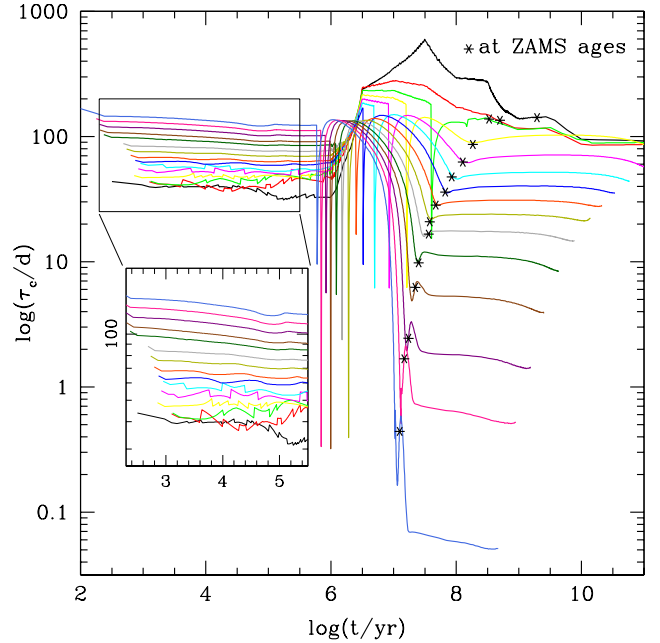


Figure 10. As Fig. 2 but extended to include τ_c obtained with our alternative location described in Section 3 for models in which $r_{\text{std}} > R_{\text{star}}$. The insert shows in detail the temporal evolution of τ_c during the beginning of the pre-MS phase.

ear fits, for different age intervals, excluding higher masses because they deviate more from the linear behaviour.

Fig. 11, which is similar to Fig. 3, shows the convective velocities used to calculate the τ_c shown in Fig. 10 and the ZAMS age of each mass model. In comparison with Fig. 3, Fig. 11 is extended to include v_c for models in which $r_{\text{std}} > R_{\text{star}}$. On the MS, the larger the stellar mass the larger the convective velocity. The same behaviour is found on the pre-MS, except for models with $M < 0.3 M_{\odot}$ and in the mass range 0.4 to $0.6 M_{\odot}$ for ages smaller than 10^4 yr (see the amplified view of Fig. 11). In the age range $5.5 \leq \log(t/\text{yr}) \leq 8.0$, where radiative cores form, this general correlation between v_c and age is modified essentially by the peaks in the v_c curves.

As τ_c , through its relation with Ro , plays an important role in stellar activity investigations and is closely related to the stellar mass, we parameterise our updated local convective turnover times by fitting linearly $\log(\tau_c)$ as a function of mass for each age shown in Table 1. The best fit for $\log(\tau_c/\text{d})$ at the ZAMS is

$$\log(\tau_c/\text{d}) = (-1.19 \pm 0.02) M/M_{\odot} + (2.40 \pm 0.02). \quad (2)$$

This is valid over the range $0.4 M_{\odot} \leq M \leq 1.0 M_{\odot}$. Similar parameterisations were made for the other ages shown in Table 1. Table 3 shows details of all these linear fits.

5 APPLICATIONS AND COMPARISONS WITH OBSERVATIONS

In order to test our theoretical convective turnover times, we used them to calculate the Rossby number of 847 stars, 824 from the sample of Wright et al. (2011) and 23 slowly rotating fully convective stars from that of Wright et al. (2018) including those 4 from Wright & Drake (2016). First, we estimated a mass and an age for all stars, using as many of stellar parameters given by Wright et al. (2011) as possible and observational data from Wright et al. (2018).

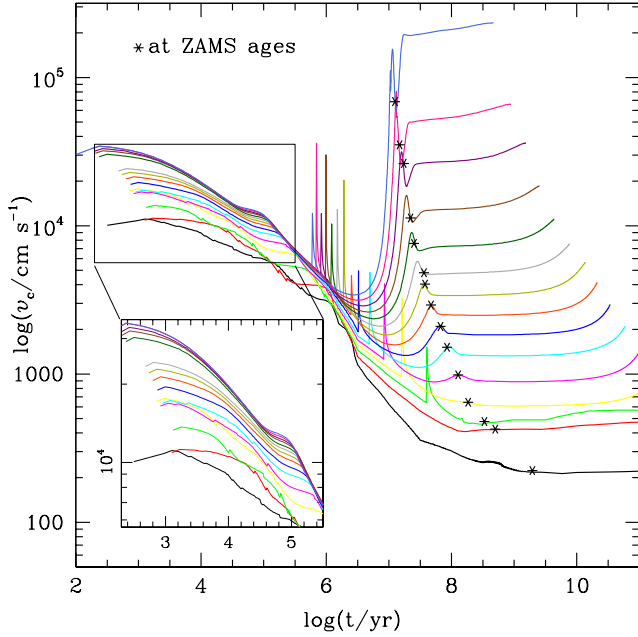


Figure 11. Same as in Fig. 3 but extended to include v_c obtained with our alternative location described in Section 3 for models in which $r_{\text{std}} > R_{\text{star}}$. The insert shows in detail the temporal evolution of v_c during the beginning of the pre-MS phase.

Table 3. Details of linear fits with the equation $\tau_c = AM/M_\odot + B$. Column 1 gives the logarithm of stellar age, col. 2 the mass range used in the fits (the same used in Table 1), col. 3 the coefficient A and col. 4 the coefficient B.

log(t/yr)	Mass range M_\odot	coefficient A	coefficient B
6.00	1.3 to 1.5	0.6 ± 0.2	1.3 ± 0.2
6.50	0.9 to 1.5	-0.30 ± 0.03	2.41 ± 0.03
7.00	0.6 to 1.2	-0.78 ± 0.05	2.67 ± 0.04
7.50	0.4 to 0.9	-1.4 ± 0.2	2.8 ± 0.1
8.00	0.4 to 1.2	-1.5 ± 0.1	2.58 ± 0.08
8.50	0.4 to 1.2	-1.4 ± 0.1	2.58 ± 0.09
9.00	0.4 to 1.1	-1.36 ± 0.05	2.54 ± 0.04
9.50	0.4 to 1.1	-1.41 ± 0.07	2.57 ± 0.05
10.00	0.4 to 1.0	-1.26 ± 0.07	2.47 ± 0.05
10.14	0.4 to 0.9	-1.36 ± 0.05	2.53 ± 0.03
ZAMS	0.4 to 1.0	-1.19 ± 0.02	2.40 ± 0.02

In this way, we minimise the impact on τ_c , besides those inherent to the way they were obtained - semi-empirically (in Wright et al. 2011, 2018) or theoretically by us. For the sample of Wright et al. (2011), we used their effective temperatures and luminosities, except for the stars for which they signalled a null luminosity and those whose positions in the HR diagram fell below our tracks. For these stars, which are mainly very low-mass, we recalculated their luminosities using the Pecaut & Mamajek (2013) V band bolometric corrections in function of $V-K$. For Wright et al. (2018)’s sample, we calculated the effective temperatures in function of $V-K$ using the colour-temperature relations of Pecaut & Mamajek (2013). Luminosities were obtained using K band bolometric corrections as a function of $V-J$ of Mann et al. (2015, 2016). In these procedures, the extinction laws of Rieke & Lebofsky (1985) were used. After estimating stellar masses and ages, we used our models, including the approach described in Section 3 for fully convective stars, to ob-

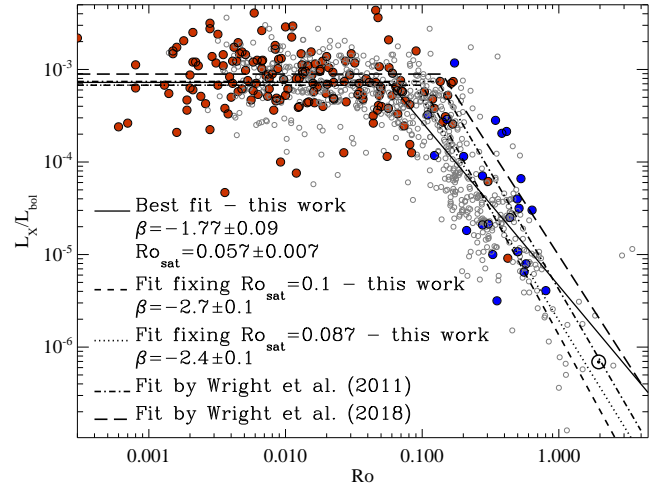


Figure 12. Fractional X-ray luminosity as a function of the Rossby number for 847 stars, 824 from Wright et al. (2011) and 23 slowly rotating fully convective stars from Wright et al. (2018). Partially convective stars are shown as grey open circles (\circ), rapidly rotating fully convective stars are shown as filled dark red circles (\bullet) and slowly rotating fully convective stars are shown as filled blue circles (\bullet). Ro was determined with our theoretical τ_c . The solid line shows our best fit to the data, the dashed line shows our fit when setting $Ro_{\text{sat}}=0.1$, the dotted line shows our fit when setting $Ro_{\text{sat}}=0.087$, the dash-dotted line shows the best fit found by Wright et al. (2011) and the long dashed line shows the best fit found by Wright et al. (2018).

tain the local convective turnover time for our stars sample. In what follows, we used our theoretical τ_c and the observed rotation periods (obtained by Wright et al. 2011, 2018) to calculate the Rossby number of each star. With our Rossby numbers and the fractional X-ray luminosities of Wright et al. (2011, 2018), we plotted these data in the L_X/L_{bol} versus Ro plane, shown in Fig. 12, to investigate the magnetic activity-rotation relationship. Symbols are the same as in Fig. 9.

We fit the distribution of stars in the rotation-activity diagram (Fig. 12) with the following two-part power-law function:

$$\frac{L_X}{L_{\text{bol}}} = \begin{cases} C Ro^\beta, & \text{if } Ro > Ro_{\text{sat}}, \\ \left(\frac{L_X}{L_{\text{bol}}} \right)_{\text{sat}}, & \text{if } Ro \leq Ro_{\text{sat}}, \end{cases} \quad (3)$$

where Ro_{sat} is the Rossby number where the saturation occurs, $(L_X/L_{\text{bol}})_{\text{sat}}$ is the mean saturation level of fractional X-ray luminosity, β the power-law slope for unsaturated stars and C a constant.

Given an initial guess for Ro_{sat} , we determined $(L_X/L_{\text{bol}})_{\text{sat}}$, which is the average of L_X/L_{bol} for $Ro \leq Ro_{\text{sat}}$. For $Ro > Ro_{\text{sat}}$, we fitted the data with a linear regression in a log-log space, keeping the constant coefficient fixed, so that the L_X/L_{bol} at Ro_{sat} is equal to $(L_X/L_{\text{bol}})_{\text{sat}}$.

Initially, following Vidotto et al. (2014) and Jackson & Jeffries (2010), we fixed $Ro_{\text{sat}}=0.1$ and the best fitting slope for the unsaturated part of the relationship was found to be $\beta=-2.7 \pm 0.1$, with a Pearson correlation coefficient $|\rho|=0.77$ and the saturation estimated to be at $\log(L_X/L_{\text{bol}})_{\text{sat}}=-3.17 \pm 0.01$ (dashed line in Fig. 12). This is consistent with what was found by Wright et al. (2018) and matches the results by Wright et al. (2011), within the error bars.

Still imposing $L_X/L_{\text{bol}} = (L_X/L_{\text{bol}})_{\text{sat}}$ at Ro_{sat} , we used a least squares method to estimate Ro_{sat} , for which the standard deviation of the data with respect to Eq. (3) reaches its minimum value. We find $Ro_{\text{sat}} = 0.057 \pm 0.009$, $\beta = -1.77 \pm 0.09$ (with $|\rho|=0.82$) and $\log(L_X/L_{\text{bol}})_{\text{sat}} = -3.14 \pm 0.02$ (solid line in Fig. 12). We then make

another least squares fit of Eq. (3) without imposing a fixed constant coefficient at Ro_{sat} . The Ro_{sat} which minimises the standard deviation agrees with the former within the errors, produces the minimum difference between the constant coefficients at Ro_{sat} , and L_X/L_{bol} at Ro_{sat} and β found in both linear regressions agree with each other within the error bars. Although this β and $\log(L_X/L_{\text{bol}})_{\text{sat}}$ is consistent with those found in the literature, Ro_{sat} is considerably smaller. Neither of these two models (solid and dashed lines in Fig. 12) fit the Sun's position (indicated with the solar symbol) in the rotation-activity diagram. For comparisons, we overplot the fits by (Wright et al. 2011, dash-dotted line) and (Wright et al. 2018, long dashed line), both described in Fig. 9.

Next, by imposing $L_X/L_{\text{bol}} = (L_X/L_{\text{bol}})_{\text{sat}}$ at Ro_{sat} in Eq. 3, we made a least squares fit to the data by fixing Ro_{sat} at a value which offers the best fit to the Sun. By using the minimum and maximum values of the solar rotation period from Donahue et al. (1996), we obtained a saturation Rossby number of $Ro_{\text{sat}} = 0.087 \pm 0.006$. This fit is the dotted line in Fig. 12 and provides $\beta = -2.4 \pm 0.1$ (with $|\rho| = 0.79$) and $\log(L_X/L_{\text{bol}})_{\text{sat}} = -3.17 \pm 0.01$. This is consistent with what is found in the literature, with β matching that of Wright et al. (2018) within the error bars. This fit is more reliable and more well-founded than the two previous fits. Besides offering a better prediction to the solar magnetic activity level, it provides a power-law index in excellent agreement with that obtained by Wright et al. (2018) who analysed the same sample of stars. Furthermore, this Ro_{sat} is still smaller than those found by Wright et al. (2011, 2018) but greater than we previously obtained with our best-fitting. It is still unclear what causes saturation in the activity-rotation relationship, but one possible explanation is that the saturation parameter Ro_{sat} is related to the stellar dynamo efficiency and that the coronal saturation originates from saturation of the dynamo. In that case, finding a smaller Ro_{sat} can imply that the dynamo process saturates at a higher dynamo number ($N_D \propto Ro^{-2}$).

Finally, we separated our sample in two subgroups, partly and fully convective stars, and fitted the data with the same Ro_{sat} used before. The fit parameters found for both subgroups agree with each other and are consistent with those found for the whole sample. This indicates that totally and partially convective stars seem to operate dynamos that cannot be distinguished through the analysis of their rotation-activity relationships. In such a scenario, the tachocline would not be an essential ingredient to the dynamo and the combined effects of differential rotation and the Coriolis force would be enough to amplify the magnetic field. Although it is believed that large-scale magnetic fields would not settle in convective zones, recent MHD simulations without a tachocline have given rise to stable magnetic structures (Brown et al. 2010).

6 CONCLUSIONS

We present a new set of pre-MS and MS evolutionary tracks, including Rossby numbers, global and local convective turnover times in the mass range of 0.1 to $1.5 M_{\odot}$. Aiming to overcome a problem concerning the location where τ_c should be theoretically determined by evolutionary models of fully convective stars (for which the standard location, $r_{\text{std}} = \ell/2$ above the base of the convective zone, is not appropriate, because then $r_{\text{std}} > R_{\text{star}}$), we performed computations of τ_c for models with $M \geq 0.4 M_{\odot}$ throughout the whole convective zone of the stars for some selected stellar ages. Profiles of Ro , τ_c and v_c are very steep near the centre and the surface of the star but they are less steep at intermediate stellar radii. Then, for each selected age, we identified r_{std} in these models and made a linear fit to these

positions (in units of H_p) as a function of stellar mass. We also parameterise τ_c as a function of mass for the same stellar ages. When extrapolated to lower masses ($M < 0.4 M_{\odot}$), our predicted locations of where τ_c should be calculated follow the same trend exhibited by models with $M \geq 0.4 M_{\odot}$. I.e., they are supposed to be found near the less steep region of the respective profiles. This suggests that our method is a promising approach.

Next, we introduced $r_{\text{std}}/H_p(M, \text{age})$, our alternative location to calculate τ_c , in models for which $r_{\text{std}} > R_{\text{star}}$ in the ATON code. This allowed estimating τ_c for fully convective stars. At the beginning of the pre-MS, τ_c is roughly constant and increases with the stellar mass. It presents a large variation before reaching the MS and then remains nearly constant again, with τ_c increasing with decreasing mass. The convective velocity decreases in the beginning of the pre-MS and the larger the stellar mass the larger the convective velocity. It varies significantly before reaching the MS and remains almost constant after that. On the MS v_c increases with the stellar mass.

Our evolutionary tracks were used to estimate stellar masses, ages and local convective turnover times of stars from the samples of Wright et al. (2011, 2018). We plotted them in the rotation-activity diagram, which presents two main different regions, saturated and unsaturated. We fitted the data in these two regions with a two-part power-law function by three different methods. By considering the fit which reproduces the Sun's position, we found $Ro_{\text{sat}} = 0.087 \pm 0.006$, $\log(L_X/L_{\text{bol}})_{\text{sat}} = -3.17 \pm 0.01$ and the inclination of the unsaturated region was found to be $\beta = -2.4 \pm 0.1$. These are consistent with others found in the literature and β is consistent with a dynamo efficiency which scales with Ro^{-2} . According to our analysis of the rotation-activity relationship of both partially and fully convective subsamples, these operate similar dynamos, showing the same dependence of L_X/L_{bol} on Ro . This would imply that the tachocline is not a fundamental ingredient for the dynamo process.

ACKNOWLEDGEMENTS

The authors thank Drs. Francesca D'Antona (INAF-OAR, Italy) and Italo Mazzitelli (INAF-IASF, Italy) for granting them full access to the ATON evolutionary code. We also are grateful to the referee, Dr. Christopher Tout, for his many comments and suggestions that helped to improve this work. Financial support from the Brazilian agencies CAPES, CNPq and FAPEMIG is gratefully acknowledged.

DATA AVAILABILITY

The authors confirm that the observational data supporting the findings of this study were obtained by Wright et al. (2011, 2018) and that the theoretical data generated by this study are available within the article, its supplementary materials or through requests to the corresponding author.

REFERENCES

- Alecian, E., Villedun, F., Grunhut, J., Hussain, G., Neiner, C., Wade, G.A. and The BinaMicS collaboration, 2019, Proceedings of Astro Fluid 2016, edited by A.S. Brun, S. Mathis, C. Charbonnel and B. Dubrulle, EAS Publications Series, 82, 345, 355
- Alexander, D.R., Ferguson, J.W., 1994, ApJ, 437, 879
- Alexander, F., Preibisch, T., 2012, A&A, 539, A64
- Allard, F., Hauschildt, P.H., Schweitzer, A., 2000, ApJ, 539, 366

- Argiroffi, C., Caramazza, M., Micela, F., Moraux, E., and Bouvier, J., 2014, Proceedings IAU Symposium, No. 302, Magnetic Fields throughout Stellar Evolution, 2013, edited by P. Petit, M. Jardine & H. Spruit, p. 102
- Argiroffi, C., Caramazza, M., Micela, G., Sciortino, S., Moraux, E., Bouvier, J., Flaccomio, E., 2016, *A&A*, 589, A113
- Asplund, M., Grevesse, N., Sauval, A. J., Scott, P., 2009, *ARA&A*, 47, 481A
- Baraffe, I., Chabrier, G., Allard, R., Hauschildt, P.H., 1997, *A&A*, 327, 1054
- Böhm-Vitense, E., 1958, *Z. Astrophys.*, 46, 108
- Brown, B.P., Browning, M.K., Brun, A.S., Miesch, M.S., Toomre, J., *ApJ*, 711, 424
- Browning, M.K., 2008, *ApJ*, 676, 1262
- Brun, A.S., Browning, M.K., 2017, *Living Rev. Sol. Phys.* 14, 4
- Donahue, R.A., Saar, S.H., Baliunas, S.L., 1996, *ApJ*, 466, 384
- Donati, J.-F., Landstreet, J.D., 2009, *ARA&A*, 47, 333
- Durney, B.R., De Young, D.S., Roxburgh, I.W., 1993, *Sol. Phys.*, 145, 207
- Eggleton, P.P., 1971, *MNRAS*, 151, 351
- Eggleton, P.P., 1972, *MNRAS*, 156, 361
- Feiden, G.A., 2013, PhD Thesis, Dartmouth College
- Feigelson, E.D., Gaffney, J.A., Garmire, G., Hillenbrand, L.A., Townsley, L., 2003, *ApJ*, 584, 911
- Flaccomio, E., Micela, G., Sciortino, S., 2003, *A&A*, 402, 277
- Frazier, E.N., *SoPh*, 14, 89
- Gilman, P.A., 1980, in *IAU Colloquium 51, Stellar Turbulence*, ed. D. Gray and J. Linsky (New York: Springer), 114, 19
- Gilliland, R.L., 1986, *ApJ*, 300, 339
- Iglesias, C.A., Rogers, F.J., 1993, *ApJ*, 412, 752
- Jackson, R.J., Jeffries, R.D., 2010, *MNRAS*, 407, 465
- Jardine, M., Unruh, Y.C., 1999, *A&A*, 346, 883
- Jung, Y.K., Kim, Y.-C., 2007, *JASS*, 24, 1
- Kawaler, S.D., 1987, *PASP*, 99, 1322
- Keszthelyi, Z., Meynet, G., Shultz, M.E., David-Uraz, A., ud-Doula, A., Townsend, R.H.D., Wade, G. A., Georgy, C., Petit, V., Owocki, S.P. *MNRAS*, 493, 518
- Kim, Y.-C., Demarque, P.S., 1996, *ApJ*, 457, 340
- Kraft, R.P., 1967, *ApJ*, 150, 551
- Landin, N.R., Ventura, P., D'Antona, F., Mendes, L.T.S., Vaz, L.P.R., 2006, *A&A*, 456, 269
- Landin, N.R., Mendes, L.T.S., Vaz, L.P.R., 2010, *A&A*, 510, 46
- Mann, A.W., Feiden, G.A., Gaidos, E., Boyajian, T., von Braun, K., 2015, *ApJ*, 804, 64
- Mann, A.W., Feiden, G.A., Gaidos, E., Boyajian, T., von Braun, K., 2016, *ApJ*, 819, 87
- Mendes, L.T.S., D'Antona, F., Mazzitelli, I., 1999, *A&A*, 341, 174
- Mihalas, D., Dappen, W., & Hummer, D.G. 1988, *ApJ*, 331, 815
- Mohanty, S., Basri, G., 2003, *AJ*, 583, 451
- Morin, J., Donati, J.-F., Petit, P., Delfosse, X., Forveille, T., Jardine, M.M., 2010, *MNRAS*, 407, 2269
- Nelson, O.R., 2008, Ph.D. Thesis, Federal University of Rio Grande do Norte, Natal, Brazil
- Newton, E.R., Irwin, J., Charbonneau, D., Berlind, P., Calkins, M.L., and Mink, J., 2017, *ApJ*, 834, 85
- Noyes, R.W., Hartmann, S., Baliunas, S., Duncan, D.K., Vaughan A., 1984, *ApJ*, 279, 763
- Pallavicini, R., Golub, L., Rosner, R., Vaiana, G.S., Ayres, T., Linsky, J.L., 1981, *ApJ*, 248, 279
- Parker, E.N., *ApJ*, 198, 205
- Pecaut, M.J., Mamajek, E.E., 2013, *ApJS*, 208, 9
- Pizzolato, N., Maggio, A., Micela, G., Sciortino, S., and Ventura, P., 2003, *A&A*, 397, 147
- Preibisch, T., Kim, Y.C., Favata, F., Feigelson, E.D., Flaccomio, E., Getman, K., Micela, G., Sciortino, S., Stassun, K., Stelzer, B., and Zinnecker, H., 2005, *ApJ*, 160, 401
- Prosser, C.F., Randich, S., Stauffer, J.R., Schmitt, J.H.M.M. Simon, T., 1996, *AJ*, 112, 1570
- Randich, S., Schmitt, J.H.M.M., Prosser, C.F., Stauffer, J.R., 1996, *A&A*, 305, 785
- Rieke, G.H., Lebofsky, M.J., 1985, *ApJ*, 288, 618
- Rogers, F.J., Swenson, F.J., & Iglesias, C.A. 1996, *ApJ*, 456, 902
- Schatzman, E.L., Praderie, F., King, A.R., 1993, in *The Stars*, Springer-Verlag
- Skumanich, A., 1972, *ApJ*, 171, 565
- Soderblom, D.R., Stauffer, J.R., Hudon, J.D., Jones, B.F., 1993, *ApJSS*, 85, 315
- Stauffer, J.R., Caillault, J.-P., Gagné, M., Prosser, C.F., Hartmann, L.W., 1994, *ApJSS*, 91, 625
- Stępień, K., Schmitt, J.H.M.M. & Voges, W., 2001, *A&A*, 370, 157
- Thompson, M.J., Christensen-Dalsgaard, J., Miesch, M.S., Toomre, J., 2003 *ARAA*, 41, 599
- Vidotto, A.A., Gregory, S.G., Jardine, M., Donati, J.F., Petit, P., Morin, J., Folsom, C.P., Bouvier, J., Cameron, A.C., Hussain, G., Marsden, S., Waite, I.A., Fares, R., Jeffers, S., do Nascimento Jr, J.D., *MNRAS*, 441, 2361.
- Villebrun, F., Alecian, E., Hussain, G., Bouvier, J., Folsom, C.P., Lebreton, Y., Amard, L., Charbonnel, C., Gallet, F., Haemmerlé, L., Böhm, T., Johns-Krull, C., Kochukhov, O., Marsden, S.C., Morin, J., Petit, P., 2000, *A&A*, 622, 72
- Weiss, N.O., Tobias, S.M., 2000, *SSRv.*, 94, 99
- Wright, N.J., Drake, J.J., Mamajek, E.E., and Henry, W., 2011, *ApJ*, 743, 48
- Wright, N.J., Drake, J.J., 2016, *Nature*, 535, 526
- Wright, N.J., Newton, E.R., Williams, P.K.G., Drake, J.J., Yadav R.K., 2018 *MNRAS*, 479, 2351

This paper has been typeset from a $\text{\TeX}/\text{\LaTeX}$ file prepared by the author.